

# Journal of Materials Chemistry A

Materials for energy and sustainability

Accepted Manuscript

This article can be cited before page numbers have been issued, to do this please use: W. Jiang, J. Shen, Z. Peng, G. Wu, G. Yin, X. Shi and H. Yang, *J. Mater. Chem. A*, 2020, DOI: 10.1039/D0TA02725A.



This is an Accepted Manuscript, which has been through the Royal Society of Chemistry peer review process and has been accepted for publication.

Accepted Manuscripts are published online shortly after acceptance, before technical editing, formatting and proof reading. Using this free service, authors can make their results available to the community, in citable form, before we publish the edited article. We will replace this Accepted Manuscript with the edited and formatted Advance Article as soon as it is available.

You can find more information about Accepted Manuscripts in the [Information for Authors](#).

Please note that technical editing may introduce minor changes to the text and/or graphics, which may alter content. The journal's standard [Terms & Conditions](#) and the [Ethical guidelines](#) still apply. In no event shall the Royal Society of Chemistry be held responsible for any errors or omissions in this Accepted Manuscript or any consequences arising from the use of any information it contains.

## ARTICLE

# Controllable Synthesis of Ultrasmall Pd Nanocatalyst Templated by Supramolecular Coordination Cage for Highly Efficient Reductive Dehalogenation

Received 00th January 20xx,  
Accepted 00th January 20xx

DOI: 10.1039/x0xx00000x

Wei-Ling Jiang,<sup>a</sup> Ji-Chuang Shen,<sup>a</sup> Zhiyong Peng,<sup>a</sup> Gui-Yuan Wu,<sup>a</sup> Guang-Qiang Yin,<sup>b</sup> Xueliang Shi,<sup>\*a</sup> and Hai-Bo Yang<sup>a</sup>

Supported ultrasmall noble metal nanocatalysts (UNMNs) are one of the most important classes of solid materials for heterogeneous catalysis. Herein, a simple and efficient supramolecular coordination cages (SCCs) template-strategy has been developed to synthesize UNMNs with controllable size and size distribution. A series of SCCs, including  $M_2L_4$ ,  $M_4L_2$ ,  $M_6L_4$  and  $M_{12}L_{24}$ , with well-defined sizes and shapes as well as different numbers of Pd ions were designed and synthesized as templates. Subsequently, the corresponding Pd nanocatalysts of  $M_2@CMC$ ,  $M_4@CMC$ ,  $M_6@CMC$  and  $M_{12}@CMC$  were prepared by an impregnation–reduction method on the support of carboxymethylcellulose (CMC) hydrogels. It was found that the employment of SCCs as templates could not only significantly reduce the aggregation tendency of Pd nanoparticle but also play an important role in regulating their size and size distribution. For example, the analysis of the catalysts size distribution indicated that the greater number of Pd ions the cage possesses, the bigger size of the catalyst can be obtained. Moreover, with the decrease of the concentration of the template, the size of the Pd nanocatalyst also decreased obviously. Particularly, the resultant catalyst with nano-Pd loading as high as 12.63% could still maintain a narrow size distribution. Furthermore, the as-prepared Pd nanocatalyst could serve as highly efficient polychlorinated biphenyls (PCBs) degrader both in the stirred vessel and continuous flow reactor because of its excellent catalytic efficiency in reductive dehalogenation reaction under the mild conditions. In a word, the SCCs template-strategy employed in this study provides a new guideline for the preparation of size-controllable UNMNs on a variety of supports, and meanwhile with high noble metal loading and catalytic activity.

## Introduction

Supported noble metal catalysts, as an important type of heterogeneous catalysts, have demonstrated several unique advantages over their homogeneous counterparts such as the easier separation from reaction systems, the applicability to continuous flow processes, good recyclability and much better stability, which are of great importance in large-scale industrial production.<sup>1–3</sup> However, these heterogeneous catalysts sometimes display the intrinsic poor catalytic performance relative to their homogeneous counterparts, expressing particularly with regard to the activity and selectivity.<sup>4</sup> In fact, previous studies have disclosed that, in a particular supported noble metal catalyst, only the surface atoms are used to catalyze reactions, thereby revealing the size dependent catalytic activities.<sup>5</sup> To address these issues, tremendous efforts

nanocatalysts (UNMNs) with maximum metal atom-utilization efficiency.<sup>6–14</sup> Such efforts have led to some new concepts of the supported metal nanoparticle catalyst,<sup>15,16</sup> single-site heterogeneous catalyst (SSHC)<sup>17</sup> and even single-atom catalyst (SAC),<sup>18,19</sup> which have been emerging as new research frontier in catalysis community.

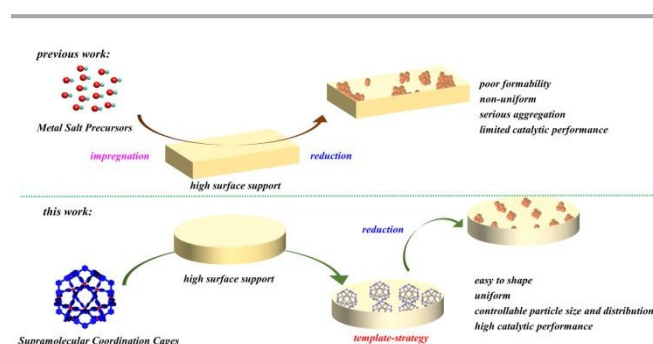


**Figure 1.** An illustrated comparison of the impregnation–reduction method between employing traditional metal salt precursors and discrete supramolecular coordination cages for preparing the UNMNs.

Generally, the prevailing strategy to design UNMNs is primarily based on the surface organometallic chemistry,<sup>20</sup> *i.e.*,

<sup>a</sup> Shanghai Key Laboratory of Green Chemistry and Chemical Processes, School of Chemistry and Molecular Engineering, East China Normal University 3663 N. Zhongshan Road, Shanghai 200062, P. R. China.  
E-mail: xlshi@chem.ecnu.edu.cn

<sup>b</sup> Department of Chemistry, University of South Florida, Tampa, Florida 33620, United States.

Electronic Supplementary Information (ESI) available: [details of any supplementary information available should be included here]. See DOI: 10.1039/x0xx00000x

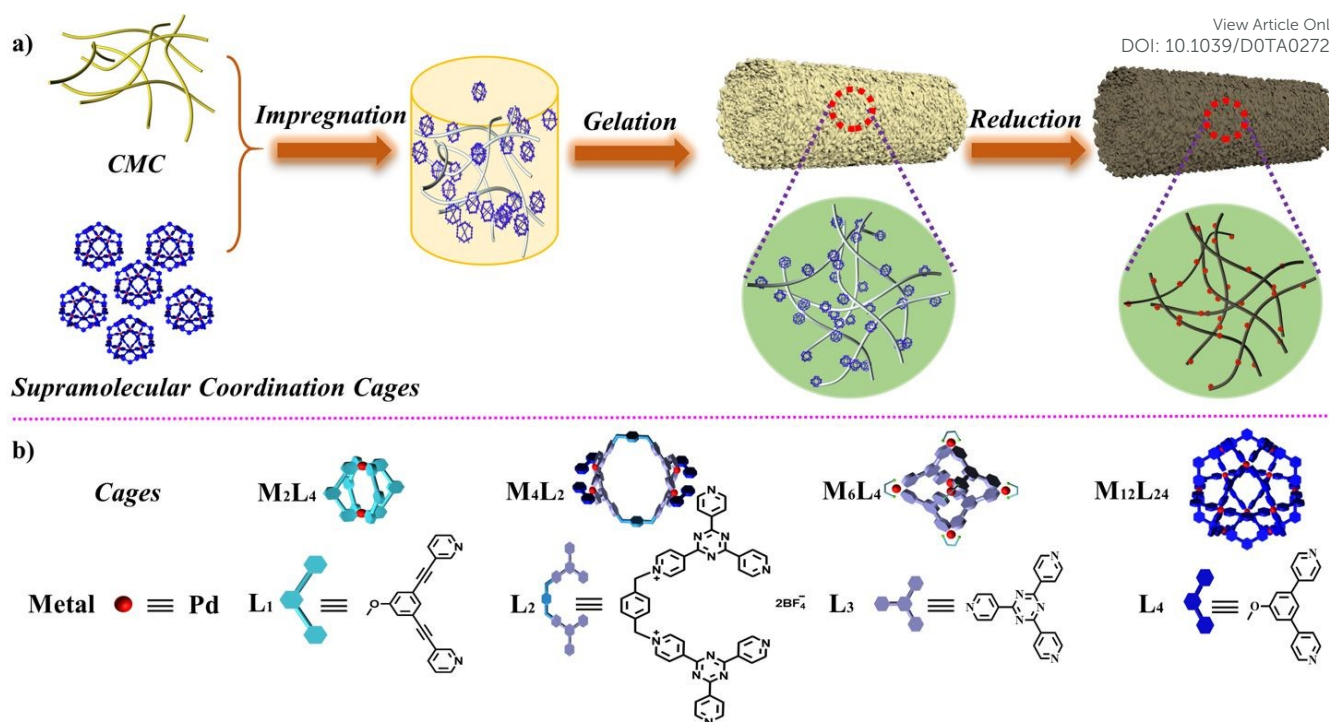
have been devoted to developing ultrasmall noble metal

impregnation and reduction of the metal precursors in a well-designed high-surface-area support such as oxides, graphene, MOFs and so on (Figure 1).<sup>21-27</sup> However, this method is likely to give rise to a broad size distribution of noble metal particles, especially under high metal precursors loading, which inevitably enhances the metallic aggregation tendency. Instead, some reports have demonstrated that the pretreatment of the metal precursors with some surface capping agents can greatly facilitate the accurate positioning metals on the supports, thus reducing the metallic aggregation tendency and resulting in the fully dispersed nanoparticles with narrow size distributions. For example, metal precursors either pre-treated with some coordinating ligands (*e.g.*, phosphine, amino and thiol), or encapsulated within dendrimers or micelles have been successfully applied to the synthesis of UNMNs, thus demonstrating distinctly unique advantages over the simple inorganic complexes' precursors.<sup>28-31</sup> Nevertheless, such surface capping agents inevitably block the catalytic sites, and decrease the activity and selectivity of the resultant UNMNs. Moreover, the removal of the surface capping agents in harsh reaction conditions sometimes leads to serious aggregation or sintering of the metallic nanoparticles/nanoclusters on the support. Besides, the achievement of scalable UNMNs with high metal contents on solid supports for practical catalytic applications still remains a synthetic challenge.<sup>28</sup> Therefore, the choice of suitable metal precursors would be essential to reduce the aggregation tendency of metallic nanoparticles, thus resulting in the UNMNs with controllable metal size and content.

Our group has a long-term interest in construction of well-defined metallosupramolecular architectures through coordination-driven self-assembly.<sup>32-37</sup> We propose herein that supramolecular coordination cages (SCCs) would be good candidate of metal precursors for the templated synthesis of the supported UNMNs (Figure 1). The rationales of such design strategy are as follows: (a) SCCs have well-defined, robust and three-dimensional (3-D) structural geometry with precise type and number of metals, which is of high importance to fine-tune the number and size distribution of metal centers in UNMNs when they function as templates; (b) the diverse bridging ligands and solid morphology of SCCs enable them to well hybrid with the support through either physical blending or reactive blending; (c) the coordination environment of the metals in SCCs is highly dynamical reversible, which makes it feasible to convert SCCs into metal nanoparticles *via* a mild reduction condition in the support.<sup>38-41</sup> Very surprisingly, although numerous well-defined SCCs have been successfully developed, up to date, very few examples on the synthesis of the supported UNMNs templated by SCCs have been reported.<sup>42,43</sup> In 2012, Fujita and co-workers first reported the preparation of hollow silica nanoparticles templated by a Pd<sub>12</sub>L<sub>24</sub> spherical complex. They claimed that the incarcerated (PdO)<sub>n</sub> and Pd<sub>n</sub> clusters were strictly controlled with  $n = ca. 12$ .<sup>42</sup> Recently, Brinker and co-workers developed a new strategy to prepare an UNMN through *in situ* reduction of Pd<sub>24</sub>L<sub>48</sub> cage confined within monosized, thiol-modified

mesoporous silica nanoparticle support.<sup>43</sup> The good catalytic performance for reduction of 4-nitrophenol and Suzuki–Miyaura coupling reaction of the resultant UNMN was also realized.<sup>43</sup> Nevertheless, in these two reports, very low concentration of the SCC precursor was able to be applied, thus leading to the relatively low noble metal loading efficiency (typical less than 5%) in the prepared UNMNs, which thereby cannot well embody the distinctive advantages of SCCs in the design of UNMNs with high catalyst loading. Therefore, the development of new UNMNs with high catalyst loading templated by SCCs is still in great need. Moreover, the relationship between the structures of SCCs and the properties of UNMNs still remains unknown due to the lack of successful UNMNs systems using different SCCs as templates. In this context, aiming to fill the research gap of this area, this Article will present the controllable synthesis of ultrasmall Pd nanocatalysts employing different SCCs as templates and explore their structure-property relationship.

Herein, a series of SCCs, including M<sub>2</sub>L<sub>4</sub>, M<sub>4</sub>L<sub>2</sub>, M<sub>6</sub>L<sub>4</sub> and M<sub>12</sub>L<sub>24</sub>, with well-defined sizes and shapes as well as different numbers of Pd ions have been designed and synthesized. In particular, different from the previous reports, the corresponding Pd nanocatalysts have been successfully prepared by an impregnation-reduction method in the support of carboxymethylcellulose (CMC) hydrogels. The results revealed a clear structure-property relationship that the employment of SCCs as templates could significantly reduce the aggregation tendency of Pd nanoparticles. Therefore, all the prepared Pd nanocatalysts exhibited narrow size distributions ranging from 0.8 ± 0.3 nm to 2.6 ± 0.3 nm. Interestingly, the analysis of the catalysts size distribution indicated that the greater number of Pd ions the SCCs have, the bigger size of the nanocatalyst can be obtained, thus highlighting the template effect of the SCCs. Moreover, with the decrease of the concentration of cage template, the size of the resultant Pd nanocatalyst also decreases obviously. Notably, the as-prepared catalyst with nano-Pd loading as high as 12.63% could still maintain a narrow size distribution, embodying the cage-template superiority as well. As a representative, the catalytic performance of M<sub>12</sub>@CMC for reductive dehalogenation has been investigated. The catalysis result showed that M<sub>12</sub>@CMC exhibited an excellent catalytic activity and selectivity for efficiently reductive dehalogenation of various aromatic halides under the mild conditions. On this foundation, a continuous flow reactor based on M<sub>12</sub>@CMC for reductive dechlorination of polychlorinated biphenyls (PCBs) has been realized, indicating the potential application in the field of PCB degradation. To the best of our knowledge, this study for the first time demonstrated that employing well-defined supramolecular coordination cages as templates could effectively regulate the size and distribution of UNMNs and consequently improve their catalytic properties and performances. We believe that the SCCs-templated synthesis strategy developed herein could be also applied to other high-surface-area supports, which thus provides new guidance to the design and construction of UNMNs.



**Scheme 1.** An illustrated comparison of the impregnation–reduction method between employing traditional metal salt precursors and discrete supramolecular coordination cages for preparing the UNMNs.

## Results and Discussion

### Synthesis

An impregnation–reduction method was employed to prepare the UNMNs. Firstly, four SCCs of  $M_2L_4$ ,  $M_4L_2$ ,  $M_6L_4$  and  $M_{12}L_{24}$  as templates were constructed through coordination-driven self-assembly. Then, an impregnation process involving a physical blending of SCCs with CMC for the gelation of cage@CMC was carried out. Finally, the SCCs were converted into Pd nanoparticles upon a mild *in-situ* reduction (**Scheme 1**). Herein, CMC was utilized as the support because of its inexpensive, biodegradable, and easily functionalized features. Moreover, CMC possesses abundant carboxylate ( $-\text{COO}^-$ ) and  $-\text{OH}$  groups, which are conducive to coordinate and stabilize Pd particles.<sup>44</sup> It should be noted that the four SCCs of  $M_2L_4$ ,  $M_4L_2$ ,  $M_6L_4$  and  $M_{12}L_{24}$  were successfully prepared from the corresponding ligand and Pd complex via the well-developed coordination-driven self-assembly approach in nearly quantitative yield,<sup>45–48</sup> and all the SCCs were well-characterized by  $^1\text{H}$  nuclear magnetic resonance ( $^1\text{H}$  NMR) and mass spectrometry (**Scheme S1** and **Figures S1–3**). The obtained SCCs were then dispersed in an aqueous solution with sonication for 30 min, and then CMC was added to the mixture with a rapid agitation by mechanical agitation for 5 h. After gelation, the SCCs were successfully impregnated into the CMC support, making for four cage@CMC aerogels of  $M_2L_4$ @CMC,  $M_4L_2$ @CMC,  $M_6L_4$ @CMC and  $M_{12}L_{24}$ @CMC with a good cage dispersion (*vide infra*). Subsequently, the obtained cage@CMC aerogels were treated with sodium borohydride ( $\text{NaBH}_4$ ), resulting in the CMC-supported Pd nanoparticles of  $M_2$ @CMC,  $M_4$ @CMC,  $M_6$ @CMC and  $M_{12}$ @CMC. As shown in **Figure 2a** and **Figure S4**, the

composites of all aerogels have foamlike appearance. Upon mixing the cage@CMC aerogels and  $\text{NaBH}_4$ , their color immediately turned from grey to gray-black, indicating the formation of Pd nanoparticles.

In order to systematically investigate the cage template effect on the size and size distribution of the designed nanoparticles, the Pd loading of  $M_2$ @CMC,  $M_4$ @CMC,  $M_6$ @CMC and  $M_{12}$ @CMC were well controlled and a series of Pd nanocatalysts were synthesized (**Table 1** and **Table S1**). From the inductively coupled plasma-atomic emission spectrometry (ICP-AES) analysis, the determined Pd concentrations (experimental value) remained almost consistent with the corresponding theoretical Pd concentrations, indicating the impregnation and reduction process are highly efficient with the neglectable cage or Pd losses. Notably, the Pd loading efficiency could reach as high as 12.63% without significant sintering of the Pd metal (**Table 1**), basically benefiting from the distinct effect of such SCCs on reducing the aggregation tendency of Pd nanoparticles (*vide infra*). For comparison, the conventional metal source of  $\text{Pd}(\text{BF}_4)_2(\text{MeCN})_2$  was also utilized to prepare the nanoparticles. However, the mixture of  $\text{Pd}(\text{BF}_4)_2(\text{MeCN})_2$  and CMC resulted in a precipitate, consequently the solid composites of  $\text{Pd}(\text{BF}_4)_2$ @CMC and  $M_1$ @CMC rather than the aerogels were obtained (**Figures S5a** and **S5b**). Such incompatible phenomenon between  $\text{Pd}(\text{BF}_4)_2(\text{MeCN})_2$  and CMC is likely a result of the coordination between carboxylic acid group in CMC and  $\text{Pd}(\text{BF}_4)_2(\text{MeCN})_2$ , thus further emphasizing the importance of SCCs in the aerogel formation.

**Table 1.** Palladium loadings of the prepared nanocatalysts as determined by ICP-AES.

Entry	Cage(mg)	CMC (mg)	Theoretic Pd (wt %)	Experimental Pd (wt %)
3.5%-M <sub>2</sub> @CMC	130	375	3.93	3.58
3.5%-M <sub>4</sub> @CMC	66	375	3.62	3.50
3.5%-M <sub>6</sub> @CMC	110	375	3.59	3.28
3.5%-M <sub>12</sub> @CMC	106	375	3.60	3.53
0.1%-M <sub>12</sub> @CMC	5	750	0.09	0.09
1.0%-M <sub>12</sub> @CMC	30	375	1.05	1.07
5.0%-M <sub>12</sub> @CMC	150	375	5.03	4.73
12.0%-M <sub>12</sub> @CMC	480	375	14.48	12.63

Sample treatment details: the aerogel sample was ground into a powder and then dried in a vacuum oven at 100 °C for 24 h. The above powder was digested with nitric acid and sulfuric acid, and then configured into an aqueous solution for testing.

### Characterization

To further investigate the details of the impregnation and reduction process, solid-state <sup>13</sup>C nuclear magnetic resonance (<sup>13</sup>C NMR) was first employed to characterize each composite (Figure 2b and Figure S6). Taking the case of M<sub>12</sub>L<sub>24</sub> as an example, CMC displayed a characteristic <sup>13</sup>C NMR spectrum with broad <sup>13</sup>C resonances at 173, 101, and 71 ppm (Figure 2b, black line), which can be well assigned according to the literature.<sup>49,50</sup> After gelation, the M<sub>12</sub>L<sub>24</sub>@CMC aerogel showed the characteristic peaks of both CMC and cage M<sub>12</sub>L<sub>24</sub> (Figure 2b, blue line), indicating the successful impregnation of SCCs into CMC. Besides, no obvious chemical shifts were observed for both CMC and M<sub>12</sub>L<sub>24</sub>, illustrating the fact that the chemical structures of CMC and SCC remained unchanged during the impregnation process. After reduction, the <sup>13</sup>C resonances of each cage were totally disappeared (Figure 2b and Figure S6, green line), implying the high efficiency of the reduction process. Similarly, Fourier-transform infrared spectroscopy (FTIR) was also applied to elucidate the identity of the above as-prepared composites (Figure 2c and Figure S7). The FTIR spectrum of the neat CMC depicted the characteristic bands at 3437 cm<sup>-1</sup>, 1601 cm<sup>-1</sup> and 1421 cm<sup>-1</sup>, resulting from O–H stretching, COO<sup>-</sup> asymmetric and symmetric stretching vibration, respectively. After simple physical impregnation, taking M<sub>12</sub>L<sub>24</sub> as an example again, the FTIR spectrum of M<sub>12</sub>L<sub>24</sub>@CMC aerogel displayed all characteristic bands of both CMC and the corresponding cage (Figure 2c, blue line). Notably,

all characteristic bands of CMC remained unchanged in M<sub>12</sub>L<sub>24</sub>@CMC, implying that no coordination interaction occurred between Pd(II) and CMC in such physical impregnation process. After reduction, the FTIR spectra of Pd nanocatalysts all showed the absence of characteristic peaks of SCCs. By comparison, both the O–H stretching band and COO<sup>-</sup> asymmetric stretching band of CMC experienced a shift in Pd nanocatalysts, confirming the existence of the obvious coordination interaction between Pd(0) and CMC (Figure 2c, green line).<sup>44,51</sup> The demonstrated coordination interaction between Pd(0) and O–H and COO<sup>-</sup> functional groups is supposed to contribute to the formation and protection of Pd nanoparticles, and then helps to control their size distributions. Thus, the FTIR results further confirmed that the SCCs have been successfully impregnated into the CMC supports and then been fully reduced to Pd nanoparticles, which was consistent with the NMR analysis.

X-ray photoelectron spectroscopy (XPS) measurements were then performed to gain the deeper insight into the change in elemental compositions and valence states of the Pd catalyst (Figure 2d and Figures S8-10). The XPS spectrum of the M<sub>12</sub>L<sub>24</sub>@CMC clearly revealed the presence of N, F and Pd elements, which originated from the corresponding cages (Figure 2d, black line). After reduction, the peaks of N or F disappeared and the spectrum only featured the characteristic peaks of O, C, Na and Pd (Figure 2d, red line). Basically, the binding energies of Pd 3d<sub>5/2</sub> in the Pd catalyst were completely different from those of Pd 3d<sub>5/2</sub> in the cage@CMC because Pd in the nanocatalyst and cage@CMC presented different valence states. Taking M<sub>12</sub>L<sub>24</sub>@CMC and M<sub>12</sub>@CMC as examples, the binding energies of Pd 3d<sub>5/2</sub> in M<sub>12</sub>L<sub>24</sub>@CMC are 343.7 and 338.4 eV, while the binding energies of Pd 3d<sub>5/2</sub> in M<sub>12</sub>@CMC are 340.5 and 335.3 eV (Figure 2d). The decrease of binding energy (~3 eV) further elucidated that Pd(II) in cage@CMC has been fully reduced to Pd(0) and anchors on CMC,<sup>44,51</sup> which is in well agreement with the above discussions. In addition, in order to facilitate the subsequent application of the material, thermogravimetric analysis (TGA) and robust measurement of M<sub>12</sub>@CMC have been carried out to test its thermostability and robustness. Impressively, the results showed that the material has good thermal stability (Figure S11) and also has an extraordinary mechanical stability and robustness supported by weight pressing and tape test (Figure S12).

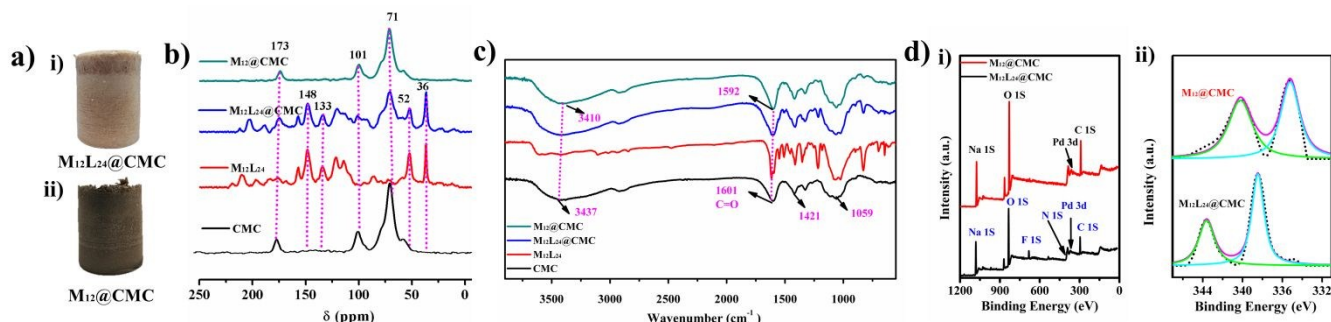


**Figure 2.** (a) The photos of aerogel of M<sub>12</sub>L<sub>24</sub>@CMC (i) and M<sub>12</sub>@CMC (ii). (b) Stacked solid-state <sup>13</sup>C NMR spectra of CMC (black), cage M<sub>12</sub>L<sub>24</sub> (red), M<sub>12</sub>L<sub>24</sub>@CMC (blue) and M<sub>12</sub>@CMC (green). (c) Stacked FT-IR spectra of CMC (black), cage M<sub>12</sub>L<sub>24</sub> (red), M<sub>12</sub>L<sub>24</sub>@CMC (blue) and M<sub>12</sub>@CMC (green). (d) XPS spectra of M<sub>12</sub>L<sub>24</sub>@CMC and M<sub>12</sub>@CMC: (i) survey spectra, (ii) high-resolution signals of Pd 3d.

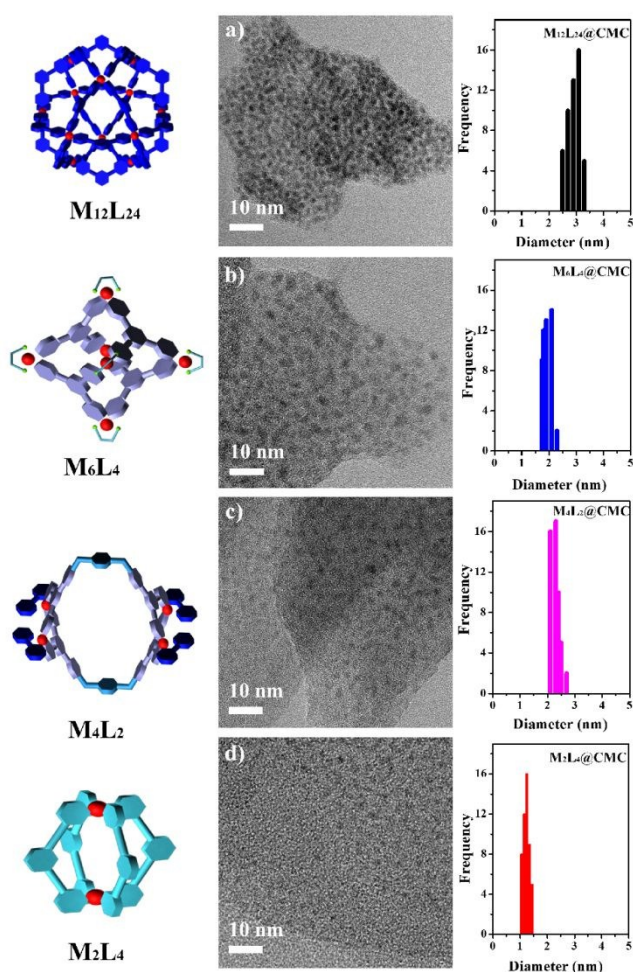


**Figure 3.** TEM images and histograms of size distributions of aerogels of (a)  $M_{12}L_{24}@CMC$ , (b)  $M_6L_4@CMC$ , (c)  $M_4L_2@CMC$  and (d)  $M_2L_4@CMC$ . The Pd concentrations of all the aerogels of cage@CMC were controlled at  $\sim 3.5\%$ .

The structure and morphology of cage@CMC aerogels and Pd nanocatalysts were then investigated by scanning electron microscopy (SEM) and transmission electron microscopy (TEM). The SEM figures demonstrated that the prepared aerogel composites before and after reduction were all microporous and highly cross linked, suggesting the fact that the reduction condition didn't destroy the CMC framework (Figure S13). The TEM images of cage@CMC aerogels revealed that the SCCs were uniformly located within the CMC support (Figure 3). The observed sizes of  $M_{12}L_{24}@CMC$ ,  $M_6L_4@CMC$ ,  $M_4L_2@CMC$  and  $M_2L_4@CMC$  were estimated to be  $2.9 \pm 0.4$ ,  $2.0 \pm 0.3$ ,  $2.4 \pm 0.3$  and  $1.2 \pm 0.2$  nm, respectively (Figure 3). The results indicated that the mean diameter of the cage@CMC presented in TEM correlated well with the calculated size of each cage (Figure S14), illustrating the highly dispersed cage in CMC. After reduction, the TEM images of the resultant CMC-supported Pd nanoparticles all showed a highly homogeneous dispersion of Pd nanocatalysts on the CMC support (Figure 4), implying that the template effectively reduced the tendency of Pd nanoparticles to undergo aggregation. In the case of the

nanocatalysts with  $\sim 3.5\%$  Pd loading on the CMC, the mean particle diameters of  $M_{12}@CMC$ ,  $M_6@CMC$ ,  $M_4@CMC$  and  $M_2@CMC$  were estimated to be  $2.4 \pm 0.3$ ,  $1.8 \pm 0.2$ ,  $1.5 \pm 0.2$  and  $0.8 \pm 0.3$  nm, respectively (Figures 4a-d). The obtained results were likely to confirm the close relationship between the particle size and the type of the coordination cage, *i.e.*, the greater number of Pd ions the cage possesses, the bigger size of the metal nanocatalyst can be obtained, thus highlighting the template effect of the SCCs. As for  $M_{12}L_{24}@CMC$  with different Pd loadings on CMC, the mean particle diameters of 12.63%, 4.73%, 1.07% and 0.09% Pd loaded catalyst were estimated to be  $2.6 \pm 0.3$ ,  $2.3 \pm 0.3$ ,  $2.0 \pm 0.3$  and  $0.9 \pm 0.4$  nm, respectively (Figures 4e-h). This indicated that with the decrease of Pd loading in CMC, the size of the metal nanocatalysts became smaller. Notably, the resulted metal nanocatalysts with a Pd loading up to 12.63% could still maintain small size with a narrow size distribution, indicating a distinct advantage of such SCC-template-strategy toward high Pd loading nanocatalyst design. The above results reveal that the size and distribution of the resultant Pd nanocatalysts are closely related to the types and concentrations of the employed cage templates. The SCCs template can not only reduce the aggregation tendency of Pd nanocatalyst but also effectively regulate their size and size distribution, which is of high importance to realize their excellent catalytic properties and performances.

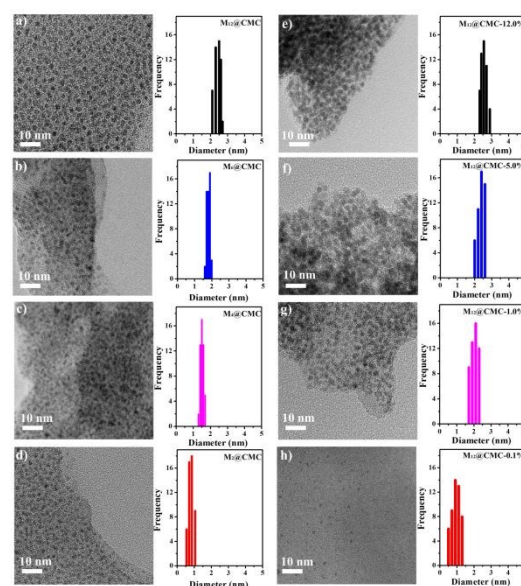


**Figure 4.** TEM images and histograms of size distributions of aerogels of Pd nanocatalysts of (a)  $M_{12}@CMC$ , (b)  $M_6@CMC$ , (c)  $M_4@CMC$ , (d)  $M_2@CMC$ , and (e-h)  $M_{12}@CMC$  with different Pd loadings. The Pd concentrations of nanocatalysts in a-d were determined at  $\sim 3.5\%$ .

**Table 2.** 12 wt%– $M_{12}@CMC$  catalyzed dechlorination reaction.

Entry	Substrate	Product	T (h)	Conversion (%)
1			6	99
2			6	97
3			6	93
4			5	99
5			1	99
6			6	98
7			6	91
8			5	99
9		/	3	92/8
10		/	22	90/10
11			10	99
12			10	99
13			15	99

Reaction conditions: chlorinated substrate (0.05 mmol), catalyst (calculating according to 5 mol% of Pd), ammonium formate (1 mmol) and methanol (4 ml) at room temperature. A mixed solvent of methanol and N, N-dimethyl formamide (V/V, 1:1) was used in entry 11-13 because of the solubility concern. <sup>a</sup>Conversion determined by GC.

### Catalytic performance

Reductive dehalogenation reaction is of paramount importance no matter from a synthetic point of view or as a destruction methodology of hazardous materials, especially in application of practical organic synthesis and degradation of organic halogenated materials.<sup>52</sup> Indeed, chemists have dedicated many efforts to this research area, and some effectively reductive dehalogenation methods including photochemical, electrochemical, microbial and radiolytic reductive methods, and so on have been well developed.<sup>53-56</sup> Among them, the supported noble metal catalysts have been demonstrated to be very effective and dominate this field, which is typically represented by the most widely used catalyst of Palladium on carbon (Pd/C).<sup>57,58</sup> Thus, the good catalytic performance for reductive dehalogenation of our prepared Pd nanoparticles is highly expected. Herein,  $M_{12}@CMC$  was applied as a representative catalyst to study the reduction dehalogenation reaction. In this work, the reductive dehalogenation is mainly based on ammonium formate-catalytic transfer hydrogenation (AF-CTH) techniques, wherein ammonium formate functions as hydrogen donor dissolving in methanol solution.<sup>59,60</sup> Firstly, a reduction of chloroaniline was carried out to examine the catalytic activity of  $M_{12}@CMC$ . It was found that the conversions were almost quantitative for the *o*, *m*, *p*-chloroaniline derivatives (Table 2, entry 1-3), indicating the

reaction is independent of the halogen position. Notably, the dechlorination of *p*-chloroaniline with  $M_{12}@CMC$  and methanol but without ammonium formate was not successful since no dechlorinated product of aniline was detected even after long duration (Figure S15). This confirms that methanol serves only as solvent and not as hydrogen donor involved in the reaction pathways. With regard to the reactivity of the halogen atom, the organic halides were reduced in the expected order of  $I > Br > Cl$  (Table S2, Figure S16), which is related to the dissociation energy of carbon-halogen bonds.<sup>61</sup> The reaction scope was then explored with a range of substituted aryl chlorides. As monitored by gas chromatography–mass spectrometry (GC-MS) analysis, all substrates were converted into the corresponding dechlorinated products in good to nearly quantitative conversions (Table S2, Table S3). Surprisingly, the substrates bearing carbonyl and nitro groups can even be further reduced to the corresponding alcohol and amine (Table 2, entry 8-10), revealing the highly catalytic activity of  $M_{12}@CMC$ . As to the multiple chlorinated substrates, mixed solvent systems of methanol/N, N-dimethyl formamide, methanol/tetrahydrofuran, and methanol/ethyl acetate were chosen to evaluate their dechlorination efficiency (Table S4, Figure S17), since the substrates were insoluble in pure methanol, made it difficult to (in-situ) detect the reactions and calculate their conversion through GC-MS analysis. The preliminary results indicated that the mixed solvent of methanol and N, N-dimethyl formamide gave a higher reaction conversion ratio (Table S4). Remarkably, the multiple chlorinated substrates could be completely dechlorinated without the formation of by-products (Table 2, entry 11-13), indicating the decent catalytic activity and selectivity in the methanol/N, N-dimethyl formamide solvent system. Moreover, the catalytic performance of  $M_{12}@CMC$  was also compared with the common commercial catalysts such as Pd/C (Table S5, Figure S18). The comparison results showed that Pd/C catalyst exhibited inferior catalytic performances including lower reaction conversion and formation of by-product, particularly in the reductive dechlorination of the multiple chlorinated substrates. Additionally, the  $M_{12}@CMC$  catalyst exhibited good reusability and could be easily recollected by simple filtration and washing. As illustrated in Figure S19, the catalyst can still maintain a high activity, and the reaction conversion could remain as much as 80% after five cycles of reaction. Moreover, no obvious sintering was observed since both the XPS survey and TEM survey of  $M_{12}@CMC$  after five cycles of reaction remained the same information with those of the freshly prepared  $M_{12}@CMC$  (Figures S20 and S21).

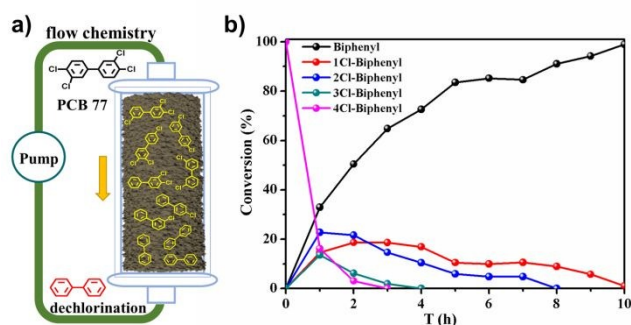


Figure 5. (a) The cartoon of the continuous-flow setup for PCB 77 degradation. (b) Degradation plot of PCB 77.

Polychlorinated biphenyls (PCBs) are a class of chlorinated organic chemicals containing 209 isomers that have been extensively used for a variety of industrial and commercial purposes for several decades. PCBs have been banned since 1976 because of the serious concerns about their degradation, bioaccumulation, chronic toxicity, which have seriously threatened humans and the environment.<sup>62-64</sup> Thus, the degradation of PCBs is one of the most enduring major issues in the field of environmental sciences. Encouraged by the results described above, we envision that our designed Pd nanocatalyst could serve as highly efficient PCBs degrader. Herein, 3,3',4,4'-tetrachlorobiphenyl (PCB 77) was selected for the degradation study. The PCB 77 degradation process by  $M_{12}@CMC$  and Pd/C was investigated first in a traditional stirred vessel. The conversion versus time curve revealed that the degradation was almost fully complete within 10 hours, and PCB 77 could be totally dechlorinated to biphenyl after 20 hours with the catalyst of  $M_{12}@CMC$  (Figure S22a). In contrast, the degradation of PCB 77 was relatively slower with the catalyst of Pd/C (Figure S22b), illustrating the superior activity of  $M_{12}@CMC$  as well. Based on these promising results, a continuous flow reactor based on the  $M_{12}@CMC$  catalyst was further designed as a demo to demonstrate its application in the removal of PCBs. The cylindrical aerogel of  $M_{12}@CMC$  was well filled into a short Teflon column (for details of the continuous flow reactor setup see Figure S23), and the cartoon of the setup and process is illustrated in Figure 5a. As expected, PCB 77 was degraded completely within 2 hours and further dechlorinated to biphenyl within 10 hours under this condition (Figure 5b, Figure S24), which manifested the high activity and unique advantages of such heterogeneous catalyst. Overall, the ultrasmall Pd nanocatalyst developed in this work may represent a versatile and efficient catalyst for the reductive dehalogenation reaction and degradation of PCB, because all reactions were carried out at room temperature in good conversion, and more importantly, with a recyclable catalyst.

## Conclusions

In summary, controllable synthesis of ultrasmall Pd nanocatalysts by using well-defined supramolecular coordination cages on a carboxymethylcellulose support has

been successfully realized, which was then employed for the efficiently reductive dehalogenation. The preliminary results revealed that the designed four supramolecular coordination cages were capable of being used as template in the efficient synthesis of cage@CMC aerogels and the corresponding Pd nanocatalysts through a simple impregnation–reduction approach. As a consequence, the coordination cages exhibited significant template effect on regulating the size and distribution of the Pd nanocatalysts, *i.e.*, the greater number of Pd ions the cage possesses, the bigger size of the catalyst can be obtained. Moreover, with the increase of the concentration of template, the size of the Pd nanocatalyst also increased obviously, while still maintaining a narrow size distribution even with a high metal loading. As a representative, the catalyst of  $M_{12}@CMC$  exhibited excellent catalytic reactivity for reductive dehalogenation of various aromatic halides. As a demo, a continuous flow reactor was further designed to demonstrate its application in the removal of PCBs. This study systematically investigated the template effect of the supramolecular coordination cage on Pd nanocatalysts preparation, and clearly revealed their structure–property relationship. We believe that the SCCs-templated synthesis strategy developed herein could be also applied to other high-surface-area supports, and helpful to the design of high metal loading single-site heterogeneous catalyst and even single-atom catalyst. Therefore, this strategy is expected to address the low catalyst loading issue in the preparation of large-scale size-controllable UNMNs for real industrial application.

## Experimental

### Synthesis of $M_4L_2$ and $M_6L_4$

$M_4L_2$  and  $M_6L_4$  were prepared according to the literatures reported from the corresponding ligand  $L_2$  and (BPy)Pd(NO<sub>3</sub>)<sub>2</sub>,  $L_3$  and (en)Pd(NO<sub>3</sub>)<sub>2</sub>.<sup>46,47</sup>

### Synthesis of $M_2L_4$

A mixture of Pd(CH<sub>3</sub>CN)<sub>2</sub>(BF<sub>4</sub>)<sub>2</sub> (44.4 mg, 0.1 mmol) and  $L_1$  (62.0 mg, 0.2 mmol) was stirred in DMSO (4 ml) at 80 °C overnight. The mixture was filtered and the crude product was precipitated by adding ether. The product was washed by CH<sub>2</sub>Cl<sub>2</sub> several times and then dried under vacuum for 12 h.

### Synthesis of $M_{12}L_{24}$

A mixture of Pd(CH<sub>3</sub>CN)<sub>2</sub>(BF<sub>4</sub>)<sub>2</sub> (44.4 mg, 0.1 mmol) and  $L_4$  (52.5 mg, 0.2 mmol) was stirred in DMSO (4 ml) at 80 °C overnight. The mixture was filtered and the crude product was precipitated by adding ether. The product was washed by CH<sub>2</sub>Cl<sub>2</sub> several times and then dried under vacuum for 12 h.

### General procedure for preparation of cage@CMC and Pd nanocatalysts

Impregnation procedure: Dried powder of cage was dispersed in aqueous solution with sonication for 30 min in a 50 mL round-bottom flask. CMC was then added to the mixture with rapid agitation by mechanical agitation (1,000 rpm) for 5 h. After that, the mixture was slowly transformed to sol, and then was poured into a cylindrical mold (3 cm in diameter and 3 cm in depth) made from PTFE (poly tetra fluoroethylene). Then the sol was soaked in acetonitrile solution until the sol was completely

transformed into a gel. The obtained gel was then pre-frozen at -19 °C overnight and freeze-dried under vacuum for 48 h, resulting in the cylinder-shape aerogel.

Reduction procedure: Pd nanocatalyst was obtained by soaking the corresponding cylinder-shape cage@CMC aerogel into the freshly prepared methanol solution of NaBH<sub>4</sub>. The mixture was stirring for 30 minutes, then washed by methanol for three times. The prepared Pd nanocatalyst was then dried under vacuum for 12 h.

#### General procedure for dechlorination reaction

The chlorinated substrate (0.05 mmol), ammonium formate (63 mg, 1.0 mmol) and 12 wt%-M<sub>12</sub>@CMC (calculating according to 5 mol% of Pd) were added to a vessel with the solvent of methanol (4 mL) or a mixed solvent of methanol and N, N-dimethyl formamide (4 mL, V/V, 1:1). Then the mixture was stirred at room temperature for several hours. The above reaction liquid was subsequently taken in the GC-MS test.

#### Continuous flow reactor for degradation of PCB 77

The reactor was designed based on a short Teflon column filled with the aerogel of M<sub>12</sub>@CMC, and the figure of the setup and process was shown in Figure S17. In the continuous flow experiment, the solution of PCB 77 (150 mg, 0.5 mmol) and

ammonium formate (630 mg, 10 mmol) in methanol/N, N-dimethyl formamide (V/V, 1:1) was continually pumped through the reaction column using a peristaltic pump with a flow rate of 1 mL/min. The reaction system was periodically detected by *in situ* GC-MS analysis.

#### Conflicts of interest

There are no conflicts to declare.

#### Acknowledgements

H.-B. Y. thanks Innovation Program of Shanghai Municipal Education Commission (No. 2019-01-07-00-05-E00012), Program for Changjiang Scholars and Innovative Research Team in University for financial support. X. S. acknowledges the financial supports sponsored by Shanghai Sailing Program (19YF1412900) and the Fundamental Research Funds for the Central Universities. W.-L. J acknowledges the ECNU Academic Innovation Promotion Program for Excellent Doctoral Students (YBNLTS2019-009).

#### References

- M. Flytzani-Stephanopoulos and B. C. Gates, *Annu. Rev. Chem. Biomol. Eng.*, 2012, **3**, 545.
- A. T. Bell, *Science*, 2003, **299**, 1688.
- N. Mizuno and M. Misono, *Chem. Rev.*, 1998, **98**, 199.
- X. Cui, W. Li, P. Ryabchuk, K. Junge and M. Beller, *Nat. Catal.*, 2018, **1**, 385.
- C. Copéret, M. Chabanas, R. P. Saint-Arroman and J. M. Basset, *Angew. Chem. Int. Ed.*, 2003, **42**, 156.
- X.-B. Fan, S. Yu, H.-L. Wu, Z.-J. Li, Y.-J. Gao, X.-B. Li, L.-P. Zhang, C.-H. Tung and L.-Z. Wu, *J. Mater. Chem. A*, 2018, **6**, 16328.
- Z. Guo, C. Xiao, R. V. Maligal-Ganesh, L. Zhou, T. W. Goh, X. Li, D. Tesfagaber, A. Thiel and W. Huang, *ACS Catal.*, 2014, **4**, 1340.
- S. Yao, X. Zhang, W. Zhou, R. Gao, W. Xu, Y. Ye, L. Lin, X. Wen, P. Liu, B. Chen, E. Crumlin, J. Guo, Z. Zuo, W. Li, J. Xie, Li Lu, C. J. Kiely, L. Gu, C. Shi, J. A. Rodriguez and D. Ma, *Science*, 2017, **357**, 389.
- M. Dhiman, B. Chalkeb and V. Polshettiwar, *J. Mater. Chem. A*, 2017, **5**, 1935.
- H. Yang, S. J. Bradley, X. Wu, A. Chan, G. I. N. Waterhouse, T. Nann, J. Zhang, P. E. Kruger, S. Ma and S. G. Telfer, *ACS Nano*, 2018, **12**, 4594.
- R. Jin, M. Peng, A. Li, Y. Deng, Z. Jia, F. Huang, Y. Ling, F. Yang, H. Fu, J. Xie, X. Han, D. Xiao, Z. Jiang, H. Liu and D. Ma, *J. Am. Chem. Soc.*, 2019, **141**, 18921.
- Bin Qi, L.-B. Di, W.-J. Xua and X.-L. Zhang, *J. Mater. Chem. A*, 2014, **2**, 11885.
- L.-B. Di, J.-S. Zhang and X.-L. Zhang, *Plasma Process. Polym.*, 2018, **15**, 1700234.
- J.-S. Zhang, H.-Y. Wang, Q. Zhao, L.-B. Di and X.-L. Zhang, *Int. J. Hydrogen Energ.*, 2020, **45**, 9624.
- N. Zheng and G. D. Stucky, *J. Am. Chem. Soc.*, 2006, **128**, 14278.
- R. J. White, R. Luque, V. L. Budarin, J. H. Clark and D. J. Macquarrie, *Chem. Soc. Rev.*, 2009, **38**, 481.
- J. M. Thomas, R. Raja and D. W. Lewis, *Angew. Chem. Int. Ed.*, 2005, **44**, 6456.
- A. Wang, J. Li and T. Zhang, *Nat. Rev. Chem.*, 2018, **2**, 65.
- H. Zhang, G. Liu, L. Shi and J. Ye, *Adv. Energy Mater.*, 2018, **8**, 1701343.
- P. Serna and B. C. Gates, *Acc. Chem. Res.*, 2014, **47**, 2612.
- E. A. Anumol, P. Kundu, P. A. Deshpande, G. Madras and N. Ravishankar, *ACS Nano*, 2011, **5**, 8049.
- S. Ji, Y. Chen, S. Zhao, W. Chen, L. Shi, Y. Wang, J. Dong, Z. Li, F. Li, C. Chen, Q. Peng, J. Li, D. Wang and Y. Li, *Angew. Chem. Int. Ed.*, 2019, **58**, 4271.
- Z. Jin, D. Nackashi, W. Lu, C. Kittrell and J. M. Tour, *Chem. Mater.*, 2010, **22**, 5695.
- M. Khan, M. N. Tahir, S. F. Adil, H. U. Khan, M. R. H. Siddiqui, A. A. Al-warthan and W. Tremel, *J. Mater. Chem. A*, 2015, **3**, 18753.
- C. Ray and T. Pal, *J. Mater. Chem. A*, 2017, **5**, 9465.
- Q. Sun, M. Chen, B. Aguila, N. Nguyen and S. Ma, *Faraday Discuss.*, 2017, **201**, 317.
- X. He, Q. He, Y. Deng, M. Peng, H. Chen, Y. Zhang, S. Yao, M. Zhang, D. Xiao, D. Ma, B. Ge and H. Ji, *Nat. Commun.*, 2019, **10**, 3663.
- R. Shen, W. Chen, Q. Peng, S. Lu, L. Zheng, X. Cao, Y. Wang, W. Zhu, J. Zhang, Z. Zhuang, C. Chen, D. Wang and Y. Li, *Chem*, 2019, **5**, 2099.
- Q.-M. Ji, J. P. Hillab and K. Ariga, *J. Mater. Chem. A*, 2013, **1**, 3600.
- R. Ye, A. V. Zhukhovitskiy, C. V. Deraedt, F. D. Toste and G. A. Somorjai, *Acc. Chem. Res.*, 2017, **50**, 1894.
- B. Liu, H. Yao, W. Song, L. Jin, I. M. Mosa, J. F. Rusling and S. L. Suib, *J. Am. Chem. Soc.*, 2016, **138**, 4718.
- L. Xu, Y.-X. Wang, L.-J. Chen and H.-B. Yang, *Chem. Soc. Rev.*, 2015, **44**, 2148.
- W. Wang, Y.-X. Wang and H.-B. Yang, *Chem. Soc. Rev.*, 2016, **45**, 2656.
- L.-J. Chen, H.-B. Yang and M. Shionoya, *Chem. Soc. Rev.*, 2017, **46**, 2555.
- L.-J. Chen and H.-B. Yang, *Acc. Chem. Res.*, 2018, **51**, 2699.
- Y. Qin, Y. Zhang, G.-Q. Yin, Y.-X. Wang, C.-W. Zhang, L.-J. Chen, H.-W. Tan, X. Li, L. Xu and H.-B. Yang, *Chin. J. Chem.*, 2019, **37**, 323.
- G.-Q. Yin, L.-J. Chen, C.-H. Wang and H.-B. Yang, *Chin. J. Chem.*, 2018, **36**, 134.
- A. J. McConnell, C. S. Wood, P. P. Neelakandan and J. R. Nitschke, *Chem. Rev.*, 2015, **115**, 7729.

- 39 M. Yoshizawa and J. K. Klosterman, *Chem. Soc. Rev.*, 2014, **43**, 1885.
- 40 Y. Takezawa and M. Shionoya, *Acc. Chem. Res.*, 2012, **45**, 2066.
- 41 R. Chakrabarty, P. S. Mukherjee and P. J. Stang, *Chem. Rev.*, 2011, **111**, 6810.
- 42 K. Takao, K. Suzuki, T. Ichijo, S. Sato, H. Asakura, K. Teramura, K. Kato, T. Ohba, T. Morita and M. Fujita, *Angew. Chem. Int. Ed.*, 2012, **51**, 5893.
- 43 W. Zhu, A. Nouredine, J. Y. Howe, J. Guo and C. J. Brinker, *Nano Lett.*, 2019, **19**, 1512.
- 44 J. Xiao, Z. Lu and Y. Li, *Ind. Eng. Chem. Res.*, 2015, **54**, 790.
- 45 A. Schmidt, V. Molano, M. Hollering, A. Pöthig, A. Casini and F. E. Kühn, *Chem. Eur. J.*, 2016, **22**, 2253.
- 46 L.-X. Cai, S.-C. Li, D.-N. Yan, L.-P. Zhou, F. Guo and Q.-F. Sun, *J. Am. Chem. Soc.*, 2018, **140**, 4869.
- 47 M. Fujita, D. Oguro, M. Miyazawa, H. Oka, K. Yamaguchi and K. Ogura, *Nature*, 1995, **378**, 469.
- 48 M. Tominaga, K. Suzuki, M. Kawano, T. Kusukawa, T. Ozeki, S. Sakamoto, K. Yamaguchi and M. Fujita, *Angew. Chem.*, 2004, **116**, 5739.
- 49 J. Liu, J. Sutton and C. B. Roberts, *J. Phys. Chem. C*, 2007, **111**, 11566.
- 50 K. R. Roshan, G. Mathai, J. Kim, J. Tharun, G. A. Parka and D. W. Park, *Green Chem.*, 2012, **14**, 2933.
- 51 F. He, D. Zhao, J. Liu and C. B. Roberts, *Ind. Eng. Chem. Res.*, 2007, **46**, 29.
- 52 F. Alonso, I. P. Beletskaya and M. Yus, *Chem. Rev.*, 2002, **102**, 4009.
- 53 J. M. R. Narayanam, J. W. Tucker and C. R. J. Stephenson, *J. Am. Chem. Soc.*, 2009, **131**, 8756.
- 54 M. Wirtz, J. Klucik and M. Rivera, *J. Am. Chem. Soc.*, 2000, **122**, 1047.
- 55 M. Bunge, L. Adrian, A. Kraus, M. Opel, W. G. Lorenz, J. R. Andreesen, H. Görisch and U. Lechner, *Nature*, 2003, **421**, 357.
- 56 C. Kunze, M. Bommer, W. R. Hagen, M. Uksa, H. Dobbek, T. Schubert and G. Diekert, *Nat. Commun.*, 2017, **8**, 15858.
- 57 X. Liu and D. Astruc, *Adv. Synth. Catal.*, 2018, **360**, 3426.
- 58 R. M. Mironenko, O. B. Belskaya and V. A. Likholobov, *Catal. Today*, 2019, DOI: 10.1016/j.cattod.2019.03.023.
- 59 M. K. Anwer, D. B. Sherman, J. G. RoneyArno and F. J. Spatola, *J. Org. Chem.*, 1989, **54**, 6, 1284.
- 60 M. K. Anwer and A. F. Spatola, *Tetrahedron Lett.*, 1985, **26**, 1381.
- 61 C. P. Andrieux, I. Gallardo, J. M. Savaent and K. B. Su, *J. Am. Chem. Soc.*, 1989, **108**, 638.
- 62 R. W. Risebrough, P. Rieche, D. B. Peakall, S. G. Herman and M. N. Kirven, *Nature*, 1968, **220**, 1098.
- 63 J. Borja, D. M. Taleon, J. Auresenia and S. Gallardo, *Process Biochem.*, 2005, **40**, 1999.
- 64 S. Safe, O. Hutzinger, *CRC Crit. Rev. Toxicol.*, 1984, **13**, 319.

View Article Online  
DOI: 10.1039/D0TA02725A

A simple and efficient supramolecular coordination cages (SCCs) template-strategy is developed to synthesize Pd nanocatalysts with controllable size and size distribution for highly efficient reductive dehalogenation.

